

1 **The statistical morphology of Saturn’s equatorial**
2 **energetic neutral atom emission**

3 **J. Kinrade^{1,*}, A. Bader^{1,*}, S. V. Badman¹, C. Paranicas², D. G. Mitchell², D.**
4 **Constable¹, C. S. Arridge¹, S. W. H. Cowley³, G. Provan³**

5 ¹Department of Physics, Lancaster University, Lancaster (UK)
6 ²Johns Hopkins University Applied Physics Laboratory, Laurel, MD (USA)
7 ³Department of Physics and Astronomy, University of Leicester, Leicester (UK)
8 *These authors contributed equally to this work

9 **Key Points:**

- 10 • We present a definitive Cassini-era picture of Saturn’s global energetic neutral atom
11 morphology using remote sensing imagery.
- 12 • Concentric tori of hydrogen and oxygen emissions are most intense at $\sim 7 - 10$
13 Saturn radii in the equatorial plane, offset towards the dayside.
- 14 • The intensity within 6–12 Saturn radii exhibits clear rotational modulation with
15 north and south magnetic phase systems.

Corresponding author: J. Kinrade, j.kinrade@lancaster.ac.uk

Abstract

Saturn's magnetosphere is an efficient emitter of energetic neutral atoms (ENAs), created through charge exchange of energetic ions with the extended neutral cloud originating from the icy moon Enceladus. We present an analysis using the complete image set captured by Cassini's Ion Neutral Camera (INCA) to characterise Saturn's average ENA morphology. Concentric tori are formed around the planet by oxygen and hydrogen ENAs, with intensity peaks between 7-10 R_S radial distance, with a $\sim 1-2 R_S$ day-side offset. Nightside intensity is brighter than the dayside, likely the result of enhancements following large-scale plasma injections from the magnetotail, and influence of the noon-midnight electric field. Global intensity is clearly modulated with the near-planetary rotation period. This Cassini-era profile of Saturn's ENA emission advances our understanding of how volcanic moons can influence plasma dynamics in giant magnetospheres and is timely ahead of the planned JUICE mission, which carries the first dedicated ENA detector to Jupiter.

Plain Language Summary

Saturn is engulfed in a cloud of neutral gas originating from ice fissures on the surface of Enceladus. Some particles collide and exchange charge, separating electrons from ions which are guided by Saturn's magnetic field. This way, Saturn's rotating magnetosphere is loaded with mass which is eventually lost into space via ejections of plasma that stretch magnetic field lines to breaking point. Some charged particles in the outer magnetosphere do not escape, but are fired back towards Saturn with field lines as they snap back into place. These energetic ions collide with neutrals, creating energetic neutral atoms (ENA) that were detectable using the INCA camera onboard Cassini. INCA's pictures of Saturn's magnetosphere reveal dynamic regions of plasma flow, important for understanding the entire system. We present an analysis of the complete INCA image set obtained over Cassini's mission, utilizing years of combined exposure to characterise Saturn's average ENA morphology. Rings of ENAs are located at distances between 7-10 R_S , where the interaction between energetic ions and the neutral cloud is largest. We also find ENA variation with Saturn's rotation period, associated with current systems that modulate the plasma sheet every ~ 10 hours.

1 Introduction

Energetic neutral atoms (ENAs) are produced by charge exchange during particle interactions between space plasmas and neutral gas populations. Remote sensing of ENAs was initially developed for probing the terrestrial magnetosphere (Roelof et al., 1985), providing the first such images of Earth's ring current region (Roelof, 1987). Since then, Cassini was the first mission to carry a dedicated ENA detector to another planet - the Ion Neutral Camera (INCA, Krimigis et al., 2004) - which successfully captured ENA emissions from the magnetospheres of Saturn and Jupiter. First detected by Voyager instruments (Kirsch et al., 1981), Saturn's ENAs have been the subject of much study during Cassini's ~ 13 year tour; the extended neutral gas cloud originating from Enceladus makes the Kronian system an efficient emitter of ENAs. Jupiter's ENA torus was observed remotely during a Cassini flyby of the Jovian system (Krimigis et al., 2002; Mauk et al., 2003) while recent studies have identified ENA signatures in particle measurements from the Jupiter Energetic-particle Detector Instrument (JEDI) onboard the Juno orbiter, revealing emissions associated with moons Io and Europa and the planet itself (Mauk, Clark, et al., 2020; Mauk, Allegrini, et al., 2020). A dedicated ENA imager is planned to fly on the JUICE mission that should arrive at Jupiter within the next decade (Grasset et al., 2013). It is therefore timely that we construct the most complete statistical morphology of Saturn's ENA emission, based on all available Cassini INCA imagery.

66 Throughout the Cassini mission, INCA imagery has helped to reveal the global plasma
 67 dynamics throughout Saturn’s magnetosphere. The neutral cloud (primarily hydrogen-
 68 and oxygen-based) extends out to at least $\sim 40 R_S$ (Melin et al., 2009) and is sustained
 69 mainly by outgassing from Enceladus, but also the planet’s rings and atmosphere. ENA
 70 production primarily occurs at radial distances from the outer edge of the E-ring/Rhea’s
 71 orbit ($\sim 8 R_S$) out to Titan’s orbit at $\sim 20 R_S$ (e.g., Carbary, Mitchell, Brandt, Roelof,
 72 & Krimigis, 2008a). Note the inherent dependence on the background neutral distribu-
 73 tion means that peak ENA intensities are not necessarily coincident with peak ion in-
 74 tensities. A significant advantage of INCA is the global views of plasma circulation pat-
 75 terns it provides, complementing the partial picture obtained through in situ particle sur-
 76 veys of Voyager (Lazarus & McNutt, 1983) and Cassini (e.g., Sergis et al., 2007; McAn-
 77 drews et al., 2009; Thomsen et al., 2014; Wilson et al., 2017).

78 Discrete, rotating regions of enhanced ENA intensity are commonly observed, interpreted
 79 as signatures of large-scale plasma injection from the magnetotail (e.g., Mitchell et al.,
 80 2005; Mitchell, Krimigis, et al., 2009; Mitchell et al., 2015; Krimigis et al., 2007). Typ-
 81 ically appearing around midnight-dawn local times near Titan’s orbit, the hot ion pop-
 82 ulation (revealed through ENA detection) drifts around the planet with $\sim 60 - 70\%$
 83 of the planetary corotation speed (Carbary, Mitchell, Brandt, Roelof, & Krimigis, 2008b;
 84 Carbary & Mitchell, 2014; Kinrade et al., 2020), eventually dispersing through charge
 85 exchange. These injection signatures sometimes persist for several planetary rotations
 86 (Paranicas et al., 2005), spreading with gradient-curvature drift (e.g., Mitchell, Krim-
 87 igis, et al., 2009) and often leading to a partial ring or spiral morphology (e.g., Brandt
 88 et al., 2008). Re-energization of existing ENA enhancements in the midnight sector can
 89 prolong their lifetime (Mitchell, Krimigis, et al., 2009). Kilometric radio (SKR) and ul-
 90 traviolet auroral signatures have been observed simultaneously with rotating ENA en-
 91 hancements (e.g., Mitchell, Krimigis, et al., 2009; Lamy et al., 2013; Nichols et al., 2014;
 92 Kinrade et al., 2020; Palmaerts et al., 2020; Wing et al., 2020) indicating the presence
 93 of a transient field-aligned current system that links injected plasma population sources
 94 to the ionosphere; indeed these rotating signatures are a major component of Saturn’s
 95 auroral emission (Bader et al., 2019). INCA also provides a remote measure of the pe-
 96 riodicities known as planetary period oscillations (PPOs) which are present throughout
 97 Saturn’s magnetosphere (Krimigis et al., 2005; Paranicas et al., 2005; Carbary, Mitchell,
 98 Brandt, Paranicas, & Krimigis, 2008; Carbary & Mitchell, 2013), complimenting the other
 99 primary indicators of periodicity; namely in situ particle detections (e.g., Clarke et al.,
 100 2010; Arridge et al., 2011; Carbary et al., 2017; Ramer et al., 2017), magnetometer (e.g.,
 101 Andrews et al., 2012, 2019; Provan et al., 2012, 2016) and kilometric radiation measure-
 102 ments (e.g., Desch, 1982; Gurnett et al., 2009; Ye et al., 2016; Lamy, 2017).

103 Carbary, Mitchell, Brandt, Roelof, and Krimigis (2008a) provided the first statistical maps
 104 of Saturn’s ENA distribution, using equatorial projections of high latitude ($> 40^\circ$) INCA
 105 images captured across 120 days in 2007. Torus-shaped distributions were found in hy-
 106 drogen and oxygen, largely concentric with the planet and with intensity peaks at dis-
 107 tances $\sim 8-11 R_S$. These long time-based ENA averages are useful for the development
 108 of global physical models and boundary information; assimilation and inversion meth-
 109 ods can be applied to INCA imagery to reconstruct the global neutral or ion populations
 110 (Brandt et al., 2008; Dialynas et al., 2013; Roelof & Skinner, 2000).

111 In this study we present a statistical analysis of Saturn’s ENA distribution using all avail-
 112 able Cassini INCA images. We developed an algorithm to ingest and calibrate the raw
 113 data and project it into the equatorial plane, detailed in the accompanying technical re-
 114 port by Bader, Kinrade, et al. (2020). Using multi-dimensional histograms we are able
 115 to filter observations by pixel-specific parameters carrying information about observa-
 116 tion geometry and target location in fixed and rotating reference frames, and create long-
 117 term mean averages.

2 Remote sensing ENA imagery

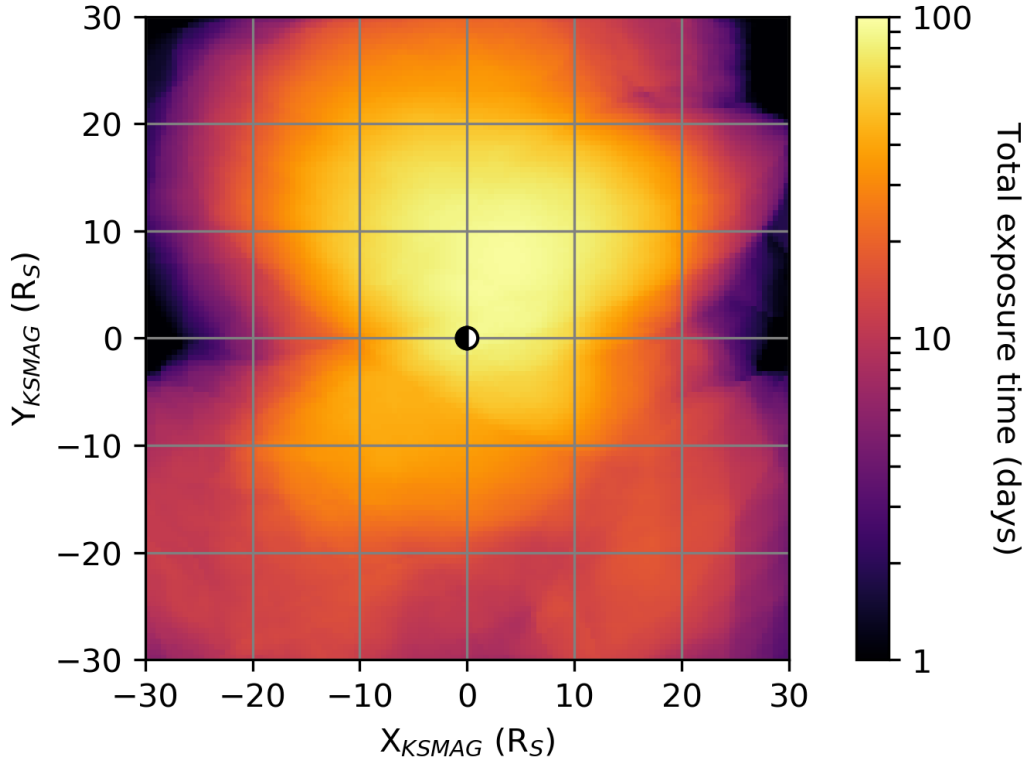


Figure 1. Map of total accumulated exposure time used for this statistical study. This is based on the sample distribution of projected pixels with LOS distance within $30 R_S$ of the spacecraft and at least 50° inclination angle. Shown is the equatorial plane of Saturn as seen from above the north pole, with the Sun located to the right. While some regions near the edges of the projection have been observed for less than a day, most pixels include tens to hundreds of days of total exposure.

119 INCA was a time of flight detector on the Cassini orbiter which investigated the Saturn
 120 system for more than a decade. It was part of the Magnetosphere IMaging Instrument
 121 (MIMI) package whose scientific goals were to study the dynamics and configuration of
 122 Saturn’s magnetosphere and its interaction with the solar wind and Saturn’s moons (Krimigis
 123 et al., 2004). Toward these goals INCA was capable of observing either ions or ENAs
 124 in keV energy ranges and determining their mass, energy and direction of motion. Its
 125 large field of view covering $120^\circ \times 90^\circ$ allowed it to measure significant parts of the ion
 126 pitch angle distribution when operated in ion mode (Mitchell, Kurth, et al., 2009; Bader,
 127 Badman, et al., 2020), or to perform global observations of ENAs in Saturn’s magneto-
 128 sphere when operated in neutral mode.

129 Over its 13+ years in orbit around Saturn, ENA observations were obtained from a vari-
 130 ety of different perspectives – the resulting dataset of ENA imagery is hence not ho-
 131 mogeneous or easy to unify. We countered this difficulty by projecting all observations
 132 into Saturn’s equatorial plane where most ENAs are created due to increased ion and
 133 neutral densities. The processing steps and the newly created dataset are described in
 134 more detail in a dedicated technical report by Bader, Kinrade, et al. (2020). Character-
 135 isation of the vertical ENA emission structure away from the magnetic/spin equator re-
 136 quires the use of a different projection routine and remains a possibility for future work.

137 In this study we use the new dataset of ENA projections to obtain long-term averages
 138 of the ENA intensity in Saturn’s equatorial plane throughout the Cassini mission. This
 139 is done by calculating histograms across the entire dataset; we bin the data by spatial
 140 location (X/Y_{KSMAG} , radial distance, local time, PPO phase, ...) and by the observed
 141 ENA intensity. The ENA intensity binning hereby covers differential ENA fluxes between
 142 10^{-15} and 10^4 particles/cm²/s/sr/keV in 380 logarithmic bins, resulting in a resolution
 143 of 20 bins per order of magnitude. Mean intensities are then calculated using the num-
 144 ber of observations in each histogram bin. As described in detail in Bader, Kinrade, et
 145 al. (2020), many projections are unsuitable for use as the viewing geometry under which
 146 they were obtained leads to pixel stretching or significant loss of resolution. Here we chose
 147 to only take into account measurements from spacecraft line-of-sight distances between
 148 $5 - 30 R_S$ from a given pixel, and from spacecraft elevations between $50 - 90^\circ$ above a
 149 given pixel. Projections showing signs of data contamination (from sunlight or ion leak-
 150 age in neutral imaging mode) were identified in Bader, Kinrade, et al. (2020) and excluded
 151 from this study.

152 Figure 1 shows the resulting total exposure time across the region of interest within the
 153 above constraints. The view is in the Saturn-centered Kronocentric Solar Magnetic (KS-
 154 MAG) frame, looking down on Saturn from above the north hemisphere with sun direc-
 155 tion to the right. This distribution is largely a function of the varying Cassini orbit ge-
 156 ometries throughout the mission; some pixel areas were observed for over 100 days in ac-
 157 cumulation, with most of the projected coverage within $20 R_S$ having at least 10 days
 158 exposure.

159 **3 Results**

160 **3.1 Mean intensity distributions**

161 Figure 2 shows the resulting maps of mean ENA intensity following our processing pro-
 162 cedure. As with Figure 1, the view is of the KSMAG equatorial plane, as seen from above
 163 the north hemisphere, with the Sun to the right of each image. Panels 2a-b show the hy-
 164 drogen 24-55 keV and 55-90 keV images, respectively, and panels 2c-d the oxygen 90-170 keV
 165 and 170-230 keV images, respectively. Note the logarithmic colour scale mapping, and
 166 the shift in scale between 2a-b and 2c-d.

167 The toroidal morphology is striking in all four cases. This is formed by a region of low-
 168 level emission near to the planet within $5 R_S$ (energetic ions are efficiently absorbed within
 169 these distances, e.g., Paranicas et al., 2008), and a ring of enhanced emission beyond this
 170 point which varies with energy (see Figure 3). The emissions are near-continuous in lo-
 171 cal time, with the intensity generally appearing brighter on the nightside than the day-
 172 side. A slight dayside offset of the tori by several R_S is also perceptible, with the emis-
 173 sion ring several Saturn radii further away from the planet than on the nightside (most
 174 clearly in the 24-55 keV hydrogen). The low level emission within $\sim 5 R_S$ may be attributed
 175 to a combination of emission from the planet (e.g., Mitchell, Krimigis, et al., 2009), spread-
 176 ing of observed intensities by the INCA point spread function (Mauk et al., 2003) and
 177 the projection procedure.

178 **3.2 Local time - distance profiles**

179 To quantify the morphology further, Figure 3 unwraps the intensity maps of Figure 2
 180 into a local time - distance frame. We have also applied Gaussian fits to each local time
 181 bin to determine the radial distance of the ENA intensity peak (black dotted line in each
 182 panel). These Gaussian fit parameters are provided in the Supplementary Information.
 183 First we see that the hydrogen ENAs peak at slightly larger radial distances ($\sim 10-13 R_S$)
 184 than the oxygen ENAs ($\sim 7-10 R_S$). These peak distance ranges are consistent with the
 185 earlier morphology study by Carbary, Mitchell, Brandt, Roelof, and Krimigis (2008a)
 186 who analysed INCA imagery from 120 days in 2007 to reveal ENA intensity peaks at $\sim 11 R_S$
 187 and $\sim 8 R_S$ for the hydrogen (20-50 keV) and oxygen (64-144 keV), respectively, albeit
 188 at slightly different energy ranges to those used here.

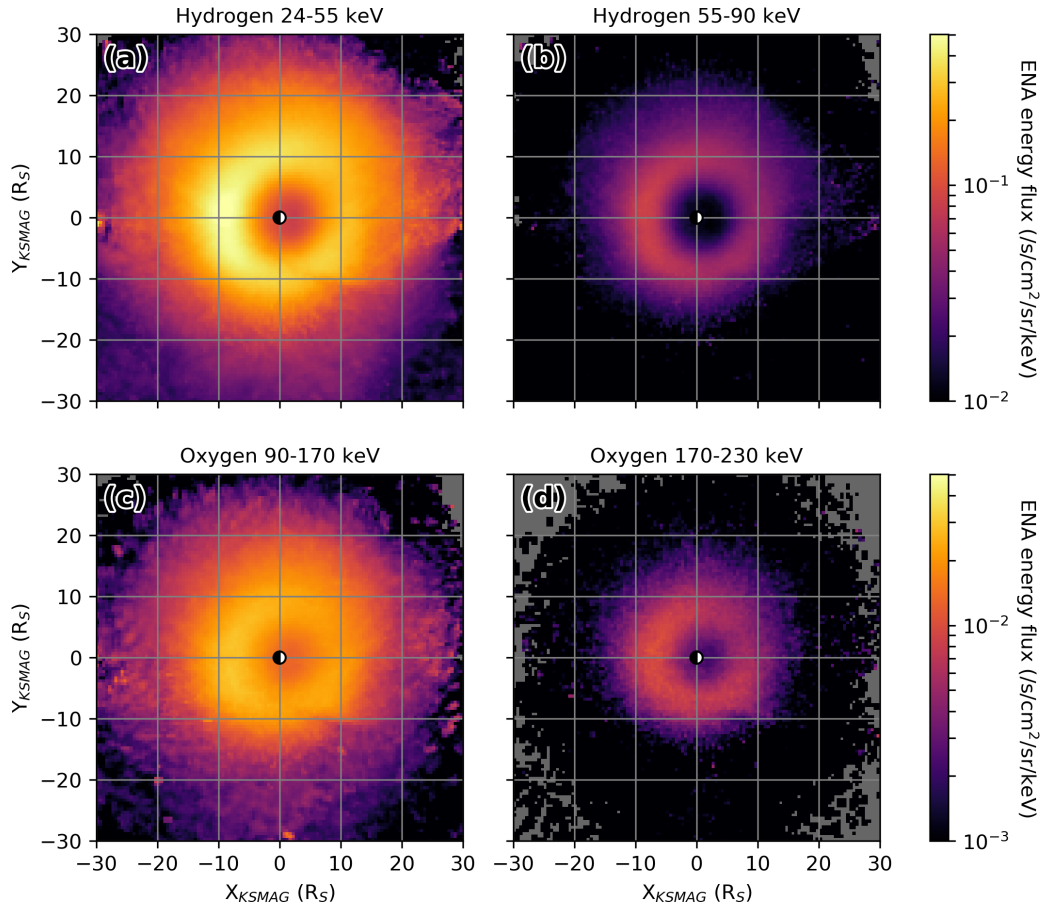


Figure 2. Maps of mean ENA intensities in the equatorial plane of Saturn for each INCA energy band. (a-b) Hydrogen 24-55 keV and 55-90 keV, respectively, and (c-d) oxygen 90-170 keV and 170-230 keV, respectively. The ring shape of the distribution is clear in all cases, with a slight position offset towards the day side and brighter intensities on the night side. Note the logarithmic colour scale mapping, and the shift in scale between (a-b) and (c-d).

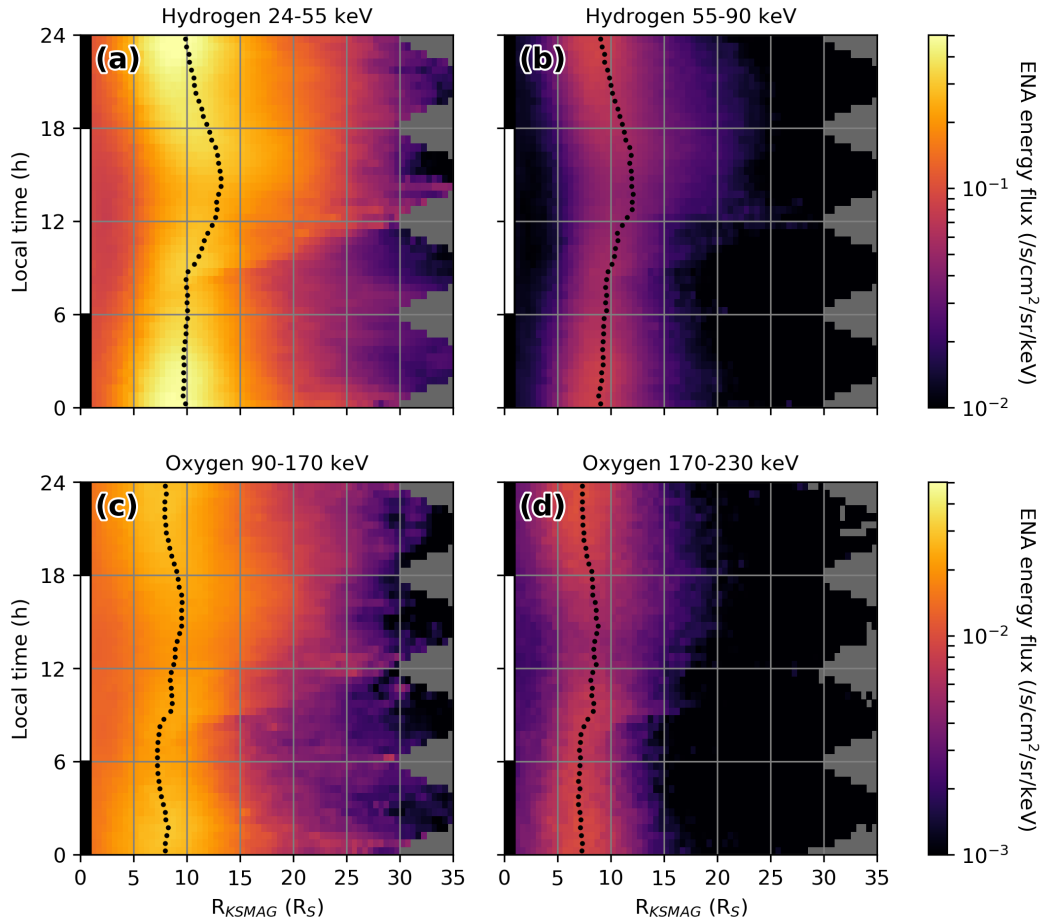


Figure 3. Mean ENA intensity in Saturn's equatorial plane in a local time and radial distance frame. (a-b) Hydrogen 24-55 keV and 55-90 keV, respectively, and (c-d) oxygen 90-170 keV and 170-230 keV, respectively. Note that different color scales apply to (a-b) and (c-d). For each local time bin, the radial intensity profile has been fitted with a Gaussian distribution to determine the radial distance of the ENA intensity peak (black dots).

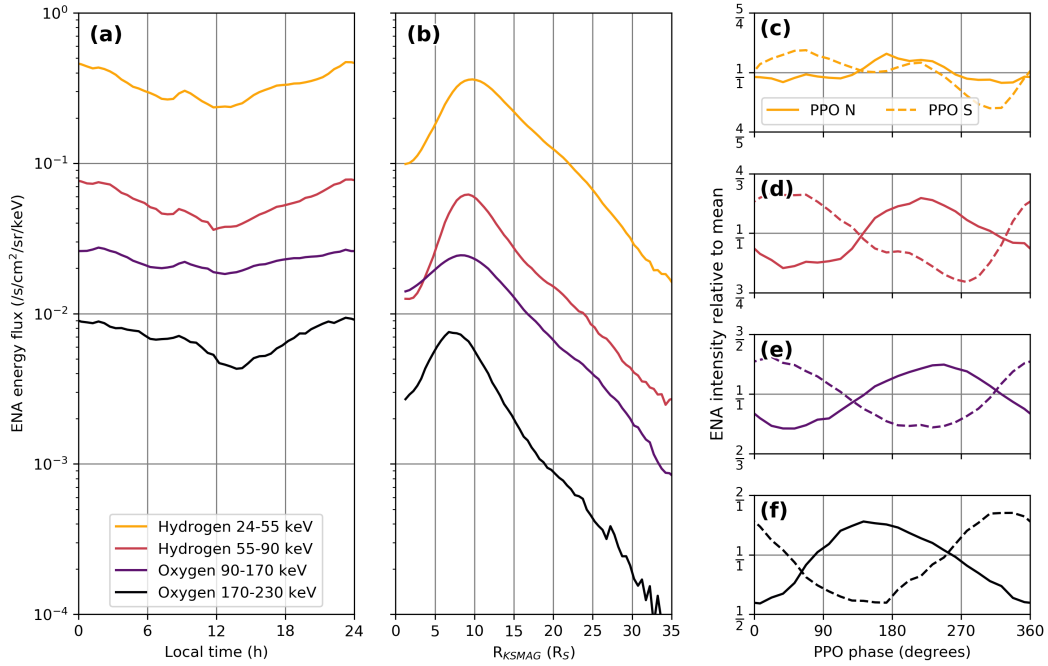


Figure 4. (a) Peak value of the average ENA intensity for each local time bin. (b) Local time-averaged radial ENA intensity profiles. (c-f) Variation of the mean ENA intensity with PPO phase. Shown is the mean ENA intensity at radial distances between 6-12 R_S on Saturn’s dayside (6-18h local time via noon) per PPO bin, relative to the overall mean ENA intensity in this region. Line colors indicate the different particle types and energy ranges as in panels (a-b); solid (dashed) lines indicate the intensity variation with northern (southern) PPO phase.

189 Second, we observe more clearly here the variation of peak distance with local time, i.e.
 190 the dayside offset of the torus apparent in Figure 2. This is clearest in the hydrogen peak
 191 fits in images 3a-b, being around $10 R_S$ on the nightside, but extending to $12-13 R_S$ on
 192 the dayside (post-noon). The offset is less clear in the oxygen distributions. This appar-
 193 ent global shift of the torus towards the dayside could be associated with the fraction
 194 of an R_S dawn-dusk trajectory shift of trapped energetic particles which has been as-
 195 sociated with the global noon-to-midnight electric field, first discovered by looking at changes
 196 in moon wake locations (e.g., Andriopoulou et al., 2012; Thomsen et al., 2012). Wilson
 197 et al. (2013), analysing in situ thermal plasma velocity and magnetic field measurements
 198 from Cassini, showed that the electric field is actually offset from the noon-midnight merid-
 199 ian by several hours local time, with the dusk-dawn drift velocity imposed on the global
 200 plasma circulation in the post-dawn direction out to at least $15 R_S$ (Wilson et al., 2017).
 201 This offset has also been observed in other data sets (e.g., Andriopoulou et al., 2014; Rous-
 202 sos et al., 2019; Sun et al., 2019) and may be produced by variation in the radial force
 203 balance at different LTs (Jia & Kivelson, 2016). This may explain why the ENA tori are
 204 offset outwards towards post-noon, signifying the point at which particles begin to re-
 205 turn inwards again in their displaced orbit. The dawn-dusk asymmetry is evident at dis-
 206 tances out to $\sim 30 R_S$ in the lower energy ENAs, suggesting that the E-field is effective
 207 at larger distances than previously considered. The offset appears to be less pronounced
 208 on the dayside for the higher energy bands, comparing the hydrogen peak fits in Figure 3a
 209 and b. This could be because the higher energy ions are less affected in their trajectory
 210 by the electric field asymmetry and thus show smaller orbital displacements, as discussed
 211 by (Thomsen et al., 2012).

212 Average local time and radial distance profiles may be extracted from Figure 3, which
 213 is what we show in Figure 4a-b for each imaging energy range. Panel 4a shows the peak
 214 value of the average intensity for each local time bin, and panel 4b shows the local-time
 215 averaged radial ENA intensity profiles. Note the logarithmic intensity scale in each case.
 216 Two general morphological trends are apparent. The ENA intensity is brighter on the
 217 nightside than the dayside (by almost half an order of magnitude), and the mean tori
 218 distance decreases with species energy (there being a $1-2 R_S$ shift between the respec-
 219 tive hydrogen and oxygen energy peaks in panel 4b). The first of these trends is likely
 220 a consequence of periodic injections of energetic plasma from Saturn’s nightside follow-
 221 ing magnetotail reconnection events which disperse as they rotate towards the dayside.
 222 The intensity asymmetry is also consistent with the effects of the noon-midnight elec-
 223 tric field, as the particle energy and differential flux decrease adiabatically when trans-
 224 ported outward on the dayside into regions of lower field strength and lower neutral den-
 225 sity. Secondly, the decrease in tori radius with increasing particle energy may be related
 226 to the penetration depth of energetic ions and their effective charge exchange cross-section
 227 which is a function of energy, i.e. higher energy ions travel further inwards radially to
 228 a region of higher neutral density before producing an ENA (e.g., Paranicas et al., 2008).
 229 Shifting energetic ions and electrons to low L-shells is considered difficult because of gradient-
 230 curvature drift out of the injection flow channels. This result may indicate that the long-
 231 term ENA picture we see is dominated by large-scale plasma flows, wider azimuthally
 232 than those typically associated with interchange processes. Oxygen ions may also be pen-
 233 etrating the inner magnetosphere at higher charge states (subject to lower gradient-curvature
 234 drift), before breaking down to lower charge states and producing ENAs (e.g., Parani-
 235 cas et al., 2020). Hao et al. (2020) recently showed that the transient noon-midnight
 236 electric field can also be responsible for accelerating electrons to the inner magnetosphere,
 237 an effect which also extends to energetic ions.

238 **3.3 Planetary period modulation**

239 Periodicity in ENAs was observed early in the Cassini mission (Krimigis et al., 2005),
 240 and was first explained by Paranicas et al. (2005) as originating from a rotating point
 241 source imposed on a constant, global ring-type emission. Carbary, Mitchell, Brandt, Parani-
 242 cas, and Krimigis (2008) then quantified the modulation periods in a Lomb-Scargle anal-

243 ysis of dawn-dusk ENA intensity variation using imagery taken from low-latitudes be-
 244 tween 2004-2007. They found that 64-144 keV oxygen ENAs exhibited strong periodic-
 245 ity around 10.8 hours, i.e. near planetary-period (specifically the period of southern PPO
 246 system which was dominant at that time), while the 20-50 keV hydrogen periodicity varied
 247 between 8-13 hours. We know from keogram track analysis of high-latitude imagery
 248 that most rotating ENA enhancements move with speeds around 60-70% corotation (e.g.,
 249 Carbary, Mitchell, Brandt, Roelof, & Krimigis, 2008b; Carbary & Mitchell, 2014; Kin-
 250 rade et al., 2020), which may explain the wider range of periodicities observed in the hy-
 251 drogen emission. So how can we test for the near planetary-period modulation of global
 252 ENA emissions?

253 Any rotational modulation of the mean global ENA intensity should result from the in-
 254 teraction of both north and south PPO current systems as they superpose in the mag-
 255 netic equator. The main effect of this interaction (in addition to north-south current sheet
 256 displacement) is modulation of the plasma sheet thickness, as the perturbation field vec-
 257 tor periodically reinforces and weakens the core field depending on phases and relative
 258 strengths of the northern and southern systems (e.g., Provan et al., 2012; Cowley et al.,
 259 2017; Thomsen et al., 2017; Bradley et al., 2018, 2020). This effect acts to minimize the
 260 thickness of the plasma sheet at PPO longitudes $\Psi_N = 0^\circ$ and $\Psi_S = 180^\circ$, when re-
 261 connection in the tail (and therefore, possibly, subsequent ENA intensification follow-
 262 ing injections) is statistically more likely to occur (Jackman et al., 2016; Bradley et al.,
 263 2018). Conversely, a thicker plasma sheet would intuitively lead to more ions interact-
 264 ing with the neutrals to produce more ENAs. Such variations in the electron density (i.e.
 265 thick and dense vs thin and tenuous) have been observed by the Cassini Langmuir Probe
 266 (Morooka et al., 2009). The thickness modulation is amplified when the north-south PPO
 267 systems superpose in antiphase, and is reduced when the systems rotate in phase rela-
 268 tive to one another.

269 Here we order all projected INCA pixels by their corresponding magnetic phase to re-
 270 veal any periodicity present in the global ENA intensity. For a given exposure time, each
 271 pixel has a magnetic longitude with respect to both the northern and southern PPO phases,
 272 and throughout the Cassini mission the N-S phase systems swept through various peri-
 273 ods of beat configuration and relative strengths. In Figure 4c-f we show the relative
 274 ENA intensities at each energy band within the main toroid region of 6-12 R_S on Sat-
 275 urn's dayside (6-18 h local time), as a fraction of the mean intensity, versus the north
 276 and south magnetic phase. We chose to only investigate dayside observations to remove
 277 noisy intensity fluctuations arising from magnetotail dynamics. Note also that local time
 278 dependence is lost when binning the pixels with respect to the rotating phase systems.

279 The sinusoidal response visible in all panels of Figure 4c-f indicates that the ENA in-
 280 tensities within the main toroid distances are being modulated within the frame of the
 281 rotating phase systems. The modulation is strongest in the 170-230 keV oxygen emis-
 282 sion (4f), the intensity varying periodically between almost double ($\sim 140^\circ$ N, $\sim 315^\circ$ S)
 283 and half ($\sim 5^\circ$ N, $\sim 175^\circ$ S) the mean level for both phase systems. The 55-90 keV hy-
 284 drogen (4d) and 90-170 keV oxygen (4e) emission responses also show clear modulation,
 285 but with a slight shift in phasing compared to higher energy oxygen. The 90-170 keV oxy-
 286 gen peaks at a northern phase of $\sim 225^\circ$, for example, compared to $\sim 140^\circ$ for the higher
 287 energy band. This higher energy phase shift is in the right direction for gradient-curvature
 288 spread of the ions to be a contributing factor, but the magnitude of the shift ($\sim 90^\circ$)
 289 seems too large for the energy difference here alone. The radial phase delay across these
 290 distances is only minor ($\sim 30^\circ$ from 9-15 R_S , Andrews et al., 2010) such that we do not
 291 expect a strong smoothing effect from averaging across the 6-12 R_S radial range. If we
 292 consider that the ENA intensifications may result from a more distant energisation and
 293 injection process then it would be appropriate to consider the retarded phase at which
 294 they originated (e.g., Bradley et al., 2018). Such an investigation is beyond the scope
 295 of the current study. The key finding is the anti-phase nature of these responses in the

north and south rotating frames, indicating that the global ENA production is affected at some level by changes in plasma sheet thickness and density driven by the rotating perturbation fields as described above. The phases where the intensity peaks occur are all around $\sim 180^\circ$ N, $\sim 0^\circ$ S, indicating maximum ENA emission from the thicker, more dense plasma sheet sector. We are unable to explain here why the strength of the rotational modulation on the ENA intensity increases with energy, but this is an interesting result that warrants further study.

4 Conclusions

We have analysed high-latitude Cassini INCA images of Saturn's equatorial ENA emission, using data from the entire mission. The result is the definitive Cassini-era picture of Saturn's equatorial ENA morphology obtained through remote sensing. The emissions are observed across four imaging bands; low and high energy hydrogen-derived ENAs (24-55 keV and 55-90 keV, respectively), and low and high energy oxygen (90-170 keV and 170-230 keV, respectively). We have used a new algorithm to sort, calibrate and project this ENA imagery into the equatorial plane for analysis, documented in Bader, Kinrade, et al. (2020). The final processed images are based on up to hundreds of days of accumulative exposure in some regions of the magnetosphere.

The long time average structure of the ENA emission is a torus around the planet, with intensity peaks at distances between 7-10 R_S (the hydrogen emission peaking $\sim 1-2 R_S$ further away from Saturn than the oxygen). This is consistent with both the inner boundary of the high particle pressure region between 8-14 R_S (e.g., Sergis et al., 2007) and where the total neutral density starts to ramp up towards the inner magnetosphere within $\sim 8 R_S$ (e.g., Cassidy & Johnson, 2010). The neutrals peak around 4 R_S near Enceladus' orbit (e.g., Richardson et al., 1998; Dialynas et al., 2013), whereas inward-travelling energetic particles of up to several hundred keV start to drop in number around L-shells of 8-9 (Paranicas et al., 2008), so the ENAs are reflecting the ion population and not just the neutral density profile. ENA intensity is generally higher on the nightside than the dayside by almost half an order of magnitude, likely the result of persistent, large-scale plasma injection activity manifesting in these long-time average pictures, and the conservation of adiabatic invariants as plasma drifts around to the dayside. Another trend common to both species and energy ranges is the radial offset of the torus towards post-noon local times by up to 3 R_S , which may be at least partly attributable to the trajectory shift experienced by trapped energetic particles under the influence of the global E-field asymmetry.

Rotational modulation of the ENA emission is clearly present within the main tori distances (6-12 R_S), given the sinusoidal pattern of mean intensity variation with both north and south magnetic phases. The 170-230 keV oxygen ENAs exhibit the strongest modulation, varying periodically between almost double and half the mean emission level. This modulation effect decreases continuously with energy, being weakest in the 24-55 keV hydrogen, for reasons yet to be explained. The phase pattern is broadly consistent across all species/energies, and indicates that periodic modulation of the plasma sheet thickness could be driving these variations in ENA production - a thicker plasma sheet would intuitively lead to higher numbers of energetic ions interacting with the neutrals to produce more ENAs.

A fall-off in projection coverage at distances around 15-20 R_S (see Figure 2) - where the main field aligned currents associated with the PPOs are thought to close in the equatorial plane (Andrews et al., 2019) - prevents us from making a robust test of the ENA intensities further out in the magnetosphere. The main ENA tori peak at distances around the possible plasmopause-like boundary identified by (Thomsen et al., 2015), a possible radial limit for injected hot plasma reaching the cooler, denser plasma of the inner magnetosphere. It may be that the modulation we observe here is driven by the combined effects of both plasma sheet thickness variation plus asymmetries in radial plasma flow

348 associated with convection patterns in the inner magnetosphere, such as those identi-
 349 fied in electron densities by Gurnett et al. (2007).

350 Characterising Saturn’s ENA distribution is useful for the development and constraint
 351 of chemistry models, and advances our understanding of how tiny volcanic moons can
 352 ultimately influence so much of the plasma dynamics in giant magnetospheres. This is
 353 particularly timely ahead of the planned JUICE explorer mission to Jupiter, which will
 354 fly with the first dedicated ENA detector to investigate the Jovian magnetosphere. Aside
 355 from being a proxy for ion loss processes, ENA imagery can be reverse-engineered to sim-
 356 ulate the background neutral population. A question yet to be fully answered is how ro-
 357 tating ENA enhancements relate to counterpart auroral emissions, and what is the na-
 358 ture of the transient current system linking them during injection activity? Future work
 359 should investigate further the nature of the periodicity apparent in the global ENA in-
 360 tensity, how this relates to large-scale plasma injection dynamics, and if this is linked
 361 to magnetotail reconnection signatures observed preferentially at certain magnetic per-
 362 turbation phases.

363 Acknowledgments

364 Cassini operations are supported by NASA (managed by the Jet Propulsion Laboratory)
 365 and the European Space Agency (ESA). All Cassini INCA data used in this study are
 366 available on NASA’s Planetary Data System (PDS) (<https://pds.jpl.nasa.gov/>), and
 367 we extend our thanks to all members of the Cassini MIMI team for their hard work. INCA
 368 ENA projections generated in this study are accessible on the Lancaster University data
 369 repository ([http://www.research.lancs.ac.uk/portal/en/datasets/cassini-inca-
 370 -equatorial-ena-projections\(e9cd8998-75ab-4fff-8e6a-9bebb74ab54b\).html](http://www.research.lancs.ac.uk/portal/en/datasets/cassini-inca-equatorial-ena-projections(e9cd8998-75ab-4fff-8e6a-9bebb74ab54b).html)).
 371 PPO phase data (2004–2017) can be found on the University of Leicester Research Archive
 372 (<http://hdl.handle.net/2381/42436>). JK, SVB and DAC were supported by STFC
 373 grant ST/R000816/1. SVB was also supported by an STFC Ernest Rutherford Fellow-
 374 ship ST/M005534/1. AB was funded by a Lancaster University FST studentship. CP
 375 would like to acknowledge grant NNX16AI46G between NASA and the Johns Hopkins
 376 University. CSA was supported by a Royal Society Research Fellowship (UF110442) and
 377 STFC grant ST/R000816/1. Work at Leicester by SWHC and GP was supported by STFC
 378 Consolidated Grant ST/N000749/1. Computations for this study were performed using
 379 the High End Computing facility at Lancaster University.

380 References

- 381 Andrews, D. J., Cowley, S. W., Provan, G., Hunt, G. J., Hadid, L. Z., Morooka,
 382 M. W., & Wahlund, J. E. (2019). The Structure of Planetary Period Os-
 383 cillations in Saturn’s Equatorial Magnetosphere: Results From the Cassini
 384 Mission. *Journal of Geophysical Research: Space Physics*, *124*(11), 8361–8395.
 385 Retrieved from [https://agupubs.onlinelibrary.wiley.com/doi/epdf/
 386 10.1029/2019JA026804](https://agupubs.onlinelibrary.wiley.com/doi/epdf/10.1029/2019JA026804) doi: 10.1029/2019JA026804
- 387 Andrews, D. J., Cowley, S. W. H., Dougherty, M. K., Lamy, L., Provan, G., &
 388 Southwood, D. J. (2012). Planetary period oscillations in Saturn’s magne-
 389 tosphere: Evolution of magnetic oscillation properties from southern sum-
 390 mer to post-equinox. *Journal of Geophysical Research: Space Physics*,
 391 *117*(4). Retrieved from [http://onlinelibrary.wiley.com/doi/10.1029/
 392 2011JA017444/abstract](http://onlinelibrary.wiley.com/doi/10.1029/2011JA017444/abstract) doi: 10.1029/2011JA017444
- 393 Andrews, D. J., Cowley, S. W. H., Dougherty, M. K., & Provan, G. (2010). Mag-
 394 netic field oscillations near the planetary period in Saturn’s equatorial mag-
 395 netosphere: Variation of amplitude and phase with radial distance and lo-
 396 cal time. *Journal of Geophysical Research: Space Physics*, *115*(A04212),
 397 1–28. Retrieved from [http://onlinelibrary.wiley.com/doi/10.1029/
 398 2009JA014729/abstract](http://onlinelibrary.wiley.com/doi/10.1029/2009JA014729/abstract) doi: 10.1029/2009JA014729

- 399 Andriopoulou, M., Roussos, E., Krupp, N., Paranicas, C., Thomsen, M., Krim-
400 igis, S., ... Glassmeier, K. H. (2012). A noon-to-midnight electric field and
401 nightside dynamics in Saturn's inner magnetosphere, using microsignature
402 observations. *Icarus*, *220*(2), 503–513. Retrieved from [http://dx.doi.org/
403 10.1016/j.icarus.2012.05.010](http://dx.doi.org/10.1016/j.icarus.2012.05.010) doi: 10.1016/j.icarus.2012.05.010
- 404 Andriopoulou, M., Roussos, E., Krupp, N., Paranicas, C., Thomsen, M., Krimigis,
405 S., ... Glassmeier, K. H. (2014). Spatial and temporal dependence of the
406 convective electric field in Saturn's inner magnetosphere. *Icarus*, *229*, 57–70.
407 Retrieved from [https://www.sciencedirect.com/science/article/pii/
408 S0019103513004570](https://www.sciencedirect.com/science/article/pii/S0019103513004570) doi: 10.1016/j.icarus.2013.10.028
- 409 Arridge, C. S., André, N., Khurana, K. K., Russell, C. T., Cowley, S. W. H., Provan,
410 G., ... Young, D. T. (2011). Periodic motion of Saturn's nightside plasma
411 sheet. *Journal of Geophysical Research: Space Physics*, *116*(A11205), 1–
412 22. Retrieved from [http://onlinelibrary.wiley.com/doi/10.1029/
413 2011JA016827/abstract](http://onlinelibrary.wiley.com/doi/10.1029/2011JA016827/abstract) doi: 10.1029/2011JA016827
- 414 Bader, A., Badman, S. V., Cowley, S. W., Yao, Z. H., Ray, L. C., Kinrade, J., ...
415 Pryor, W. R. (2019). The Dynamics of Saturn's Main Aurorae. *Geophys-
416 ical Research Letters*, *46*(17-18), 10283–10294. Retrieved from [https://
417 agupubs.onlinelibrary.wiley.com/doi/full/10.1029/2019GL084620](https://agupubs.onlinelibrary.wiley.com/doi/full/10.1029/2019GL084620) doi:
418 10.1029/2019GL084620
- 419 Bader, A., Badman, S. V., Ray, L. C., Paranicas, C. P., Lorch, C. T. S., Clark, G.,
420 ... Pryor, W. (2020). Energetic Particle Signatures Above Saturn's Auro-
421 rae. *Journal of Geophysical Research: Space Physics*, *125*(1), e2019JA027403.
422 Retrieved from [https://agupubs.onlinelibrary.wiley.com/doi/full/
423 10.1029/2019JA027403#](https://agupubs.onlinelibrary.wiley.com/doi/full/10.1029/2019JA027403#) doi: 10.1029/2019ja027403
- 424 Bader, A., Kinrade, J., Badman, S. V. B., Paranicas, C., Constable, D. A., &
425 Mitchell, D. G. (2020). A complete dataset of equatorial projections of
426 Saturn's energetic neutral atom emissions observed by Cassini-INCA. *in
427 preparation*.
- 428 Bradley, T. J., Cowley, S. W., Bunce, E. J., Melin, H., Provan, G., Nichols, J. D., ...
429 Hunt, G. J. (2020). Saturn's Nightside Dynamics During Cassini's F Ring and
430 Proximal Orbits: Response to Solar Wind and Planetary Period Oscillation
431 Modulations. *Journal of Geophysical Research: Space Physics*, *125*(9), 1–39.
432 Retrieved from [https://agupubs.onlinelibrary.wiley.com/doi/full/
433 10.1029/2020JA027907](https://agupubs.onlinelibrary.wiley.com/doi/full/10.1029/2020JA027907) doi: 10.1029/2020JA027907
- 434 Bradley, T. J., Cowley, S. W. H., Bunce, E. J., Smith, A. W., Jackman, C. M., &
435 Provan, G. (2018). Planetary Period Modulation of Reconnection Bursts
436 in Saturn's Magnetotail. *Journal of Geophysical Research: Space Physics*,
437 *123*(11), 9476–9507. Retrieved from [https://onlinelibrary.wiley.com/
438 doi/abs/10.1029/2018JA025932](https://onlinelibrary.wiley.com/doi/abs/10.1029/2018JA025932) doi: 10.1029/2018JA025932
- 439 Brandt, P. C., Paranicas, C. P., Carbary, J. F., Mitchell, D. G., Mauk, B. H.,
440 & Krimigis, S. M. (2008). Understanding the global evolution of Sat-
441 urn's ring current. *Geophysical Research Letters*, *35*(17), 1–5. Retrieved
442 from [http://onlinelibrary.wiley.com/doi/10.1029/2008GL034969/
443 full#footer-citing](http://onlinelibrary.wiley.com/doi/10.1029/2008GL034969/full#footer-citing) doi: 10.1029/2008GL034969
- 444 Carbary, J. F., & Mitchell, D. G. (2013). Periodicities in Saturn's Magneto-
445 sphere. *Reviews of Geophysics*, *51*, 1–30. Retrieved from [http://
446 onlinelibrary.wiley.com/doi/10.1002/rog.20006/abstract](http://onlinelibrary.wiley.com/doi/10.1002/rog.20006/abstract) doi:
447 doi:10.1002/rog.20006
- 448 Carbary, J. F., & Mitchell, D. G. (2014). Keogram analysis of ENA images
449 at Saturn. *Journal of Geophysical Research: Space Physics*, *119*, 1771–
450 1780. Retrieved from [http://onlinelibrary.wiley.com/doi/10.1002/
451 2014JA019784/full#references](http://onlinelibrary.wiley.com/doi/10.1002/2014JA019784/full#references) doi: 10.1002/2014JA020465.Received
- 452 Carbary, J. F., Mitchell, D. G., Brandt, P., Paranicas, C., & Krimigis, S. M.
453 (2008). ENA periodicities at Saturn. *Geophysical Research Letters*, *35*(7),

- 454 1–5. Retrieved from <http://onlinelibrary.wiley.com/doi/10.1029/2008GL033230/full#references> doi: 10.1029/2008GL033230
- 455
- 456 Carbary, J. F., Mitchell, D. G., Brandt, P., Roelof, E. C., & Krimigis, S. M.
457 (2008a). Statistical morphology of ENA emissions at Saturn. *Journal of Geophysical Research: Space Physics*, 113(5), 1–9. Retrieved from
458 <http://onlinelibrary.wiley.com/doi/10.1029/2007JA012873/epdf> doi:
459 10.1029/2007JA012873
- 460
- 461 Carbary, J. F., Mitchell, D. G., Brandt, P., Roelof, E. C., & Krimigis, S. M. (2008b).
462 Track analysis of energetic neutral atom blobs at Saturn. *Journal of Geo-*
463 *physical Research: Space Physics*, 113(1), 1–7. Retrieved from [https://](https://agupubs.onlinelibrary.wiley.com/doi/full/10.1029/2007JA012708)
464 agupubs.onlinelibrary.wiley.com/doi/full/10.1029/2007JA012708 doi:
465 10.1029/2007JA012708
- 466 Carbary, J. F., Mitchell, D. G., Kollman, P., Krupp, N., & Roussos, E. (2017). En-
467 ergetic Electron Periodicities during the Cassini Grand Finale. *Journal of Geo-*
468 *physical Research: Space Physics*, 122. Retrieved from [http://onlinelibrary](http://onlinelibrary.wiley.com/doi/10.1002/2017JA024836/full)
469 [.wiley.com/doi/10.1002/2017JA024836/full](http://onlinelibrary.wiley.com/doi/10.1002/2017JA024836/full) doi: 10.1002/2017JA024836
- 470 Cassidy, T. A., & Johnson, R. E. (2010). Collisional spreading of Ence-
471 ladus’ neutral cloud. *Icarus*, 209(2), 696–703. Retrieved from [https://](https://www.sciencedirect.com/science/article/pii/S0019103510001582#!)
472 www.sciencedirect.com/science/article/pii/S0019103510001582#! doi:
473 10.1016/j.icarus.2010.04.010
- 474 Clarke, K. E., Andrews, D. J., Arridge, C. S., Coates, A. J., & Cowley, S. W. H.
475 (2010). Magnetopause oscillations near the planetary period at Saturn: Occur-
476 rence, phase, and amplitude. *Journal of Geophysical Research: Space Physics*,
477 115(A08209). Retrieved from [https://agupubs.onlinelibrary.wiley.com/](https://agupubs.onlinelibrary.wiley.com/doi/full/10.1029/2009JA014745)
478 [doi/full/10.1029/2009JA014745](https://agupubs.onlinelibrary.wiley.com/doi/full/10.1029/2009JA014745) doi: 10.1029/2009JA014745
- 479 Cowley, S. W. H., Provan, G., Hunt, G. J., & Jackman, C. M. (2017). Plane-
480 tary period modulations of Saturn’s magnetotail current sheet: A simple
481 illustrative model. *Journal of Geophysical Research: Space Physics*, 122,
482 258–279. Retrieved from [http://onlinelibrary.wiley.com/doi/10.1002/](http://onlinelibrary.wiley.com/doi/10.1002/2016JA023367/full)
483 [2016JA023367/full](http://onlinelibrary.wiley.com/doi/10.1002/2016JA023367/full) doi: 10.1002/2017JA023993
- 484 Desch, M. D. (1982). Evidence for solar wind control of saturn radio emis-
485 sion. *Journal of Geophysical Research*, 87(A6), 4549–4554. Retrieved from
486 <http://onlinelibrary.wiley.com/doi/10.1029/JA087iA06p04549/full>
487 doi: 10.1029/JA087iA06p04549
- 488 Dialynas, K., Rymer, A. M., Mitchell, D. G., Hamilton, D. C., Krupp, N., Krim-
489 igis, S. M., & Brandt, P. C. (2013). The extended Saturnian neutral cloud
490 as revealed by global ENA simulations using Cassini/MIMI measurements.
491 *Journal of Geophysical Research: Space Physics*, 118(6), 3027–3041. Retrieved
492 from [https://agupubs.onlinelibrary.wiley.com/doi/full/10.1002/](https://agupubs.onlinelibrary.wiley.com/doi/full/10.1002/jgra.50295)
493 [jgra.50295](https://agupubs.onlinelibrary.wiley.com/doi/full/10.1002/jgra.50295) doi: 10.1002/jgra.50295
- 494 Grasset, O., Dougherty, M. K., Coustenis, A., Bunce, E. J., Erd, C., Titov, D., ...
495 Van Hoolst, T. (2013). JUper ICy moons Explorer (JUICE): An ESA mis-
496 sion to orbit Ganymede and to characterise the Jupiter system. *Planetary*
497 *and Space Science*, 78, 1–21. Retrieved from [http://dx.doi.org/10.1016/](http://dx.doi.org/10.1016/j.pss.2012.12.002)
498 [j.pss.2012.12.002](http://dx.doi.org/10.1016/j.pss.2012.12.002) doi: 10.1016/j.pss.2012.12.002
- 499 Gurnett, D. A., Lecacheux, A., Kurth, W. S., Persoon, A. M., Groene, J. B.,
500 Lamy, L., ... Carbary, J. F. (2009). Discovery of a north-south asymme-
501 try in Saturn’s radio rotation period. *Geophysical Research Letters*, 36(16),
502 2–5. Retrieved from [http://onlinelibrary.wiley.com/doi/10.1029/](http://onlinelibrary.wiley.com/doi/10.1029/2009GL039621/full)
503 [2009GL039621/full](http://onlinelibrary.wiley.com/doi/10.1029/2009GL039621/full) doi: 10.1029/2009GL039621
- 504 Gurnett, D. A., Persoon, A. M., Kurth, W. S., Groene, J. B., Averkamp, T. F.,
505 Dougherty, M. K., & Southwood, D. J. (2007). The variable rotation period
506 of the inner region of Saturn’s plasma disk. *Science*, 316(5823), 442–445. Re-
507 trieved from <https://science.sciencemag.org/content/316/5823/442> doi:
508 10.1126/science.1138562

- 509 Hao, Y.-X., Sun, Y.-X., Roussos, E., Liu, Y., Kollmann, P., Yuan, C.-J., ...
 510 Zong, Q.-G. (2020). The Formation of Saturn's and Jupiter's Electron
 511 Radiation Belts by Magnetospheric Electric Fields. *The Astrophysical*
 512 *Journal*, 905(1), L10. Retrieved from [http://dx.doi.org/10.3847/](http://dx.doi.org/10.3847/2041-8213/abca3f)
 513 [https://iopscience.iop.org/article/10.3847/](https://iopscience.iop.org/article/10.3847/2041-8213/abca3f/meta?casa_token=MjFtr9ZINh4AAAAA:aCYgQjmmmH-_ptcrUuVfjR43wSXFQBCa0k78_58h40VbbYKHvaSGPoC_-qv3F-Ea46TRr1DbA)
 514 [2041-8213/abca3f/meta?casa_token=MjFtr9ZINh4AAAAA:aCYgQjmmmH_](https://iopscience.iop.org/article/10.3847/2041-8213/abca3f/meta?casa_token=MjFtr9ZINh4AAAAA:aCYgQjmmmH-_ptcrUuVfjR43wSXFQBCa0k78_58h40VbbYKHvaSGPoC_-qv3F-Ea46TRr1DbA)
 515 [_ptcrUuVfjR43wSXFQBCa0k78_58h40VbbYKHvaSGPoC_-qv3F-Ea46TRr1DbA](https://iopscience.iop.org/article/10.3847/2041-8213/abca3f/meta?casa_token=MjFtr9ZINh4AAAAA:aCYgQjmmmH-_ptcrUuVfjR43wSXFQBCa0k78_58h40VbbYKHvaSGPoC_-qv3F-Ea46TRr1DbA)
 516 doi: 10.3847/2041-8213/abca3f
- 517 Jackman, C. M., Provan, G., & Cowley, S. W. H. (2016). Reconnection events in
 518 Saturn's magnetotail: Dependence of plasmoid occurrence on planetary period
 519 oscillation phase. *Journal of Geophysical Research A: Space Physics*, 121(4),
 520 2922–2934. Retrieved from [https://agupubs.onlinelibrary.wiley.com/](https://agupubs.onlinelibrary.wiley.com/doi/full/10.1002/2015JA021985)
 521 [doi/full/10.1002/2015JA021985](https://agupubs.onlinelibrary.wiley.com/doi/full/10.1002/2015JA021985) doi: 10.1002/2015JA021985
- 522 Jia, X., & Kivelson, M. G. (2016, feb). Dawn-dusk asymmetries in rotat-
 523 ing magnetospheres: Lessons from modeling Saturn. *Journal of Geo-*
 524 *physical Research: Space Physics*, 121(2), 1413–1424. Retrieved from
 525 <https://onlinelibrary.wiley.com/doi/abs/10.1002/2015JA021950> doi:
 526 10.1002/2015JA021950
- 527 Kinrade, J., Badman, S. V., Paranicas, C., Mitchell, D. G., Arridge, C. S., Gray,
 528 R. L., ... Achilleos, N. (2020). Tracking Counterpart Signatures in Saturn's
 529 Auroras and ENA Imagery During Large-Scale Plasma Injection Events. *Jour-*
 530 *nal of Geophysical Research: Space Physics*, 125, e2019JA027542. Retrieved
 531 from [https://agupubs.onlinelibrary.wiley.com/doi/full/10.1029/](https://agupubs.onlinelibrary.wiley.com/doi/full/10.1029/2019JA027542)
 532 [2019JA027542](https://agupubs.onlinelibrary.wiley.com/doi/full/10.1029/2019JA027542) doi: 10.1029/2019JA027542
- 533 Kirsch, E., Krimigis, S. M., Ip, W. H., & Gloeckler, G. (1981). X-ray and energetic
 534 neutral particle emission from Saturn's magnetosphere. *Nature*, 292(5825),
 535 718–721. Retrieved from <https://www.nature.com/articles/292718a0> doi:
 536 10.1038/292718a0
- 537 Krimigis, S. M., Mitchell, D. G., Hamilton, D. C., Dandouras, J., Armstrong,
 538 T. P., Bolton, S. J., ... Williams, D. J. (2002). A nebula of gases from
 539 Io surrounding Jupiter. *Nature*, 415(6875), 994–996. Retrieved from
 540 <https://www.nature.com/articles/415994a> doi: 10.1038/415994a
- 541 Krimigis, S. M., Mitchell, D. G., Hamilton, D. C., Krupp, N., Livi, S., Roelof, E. C.,
 542 ... Woch, J. (2005). Dynamics of Saturn's magnetosphere from MIMI dur-
 543 ing Cassini's orbital insertion. *Science*, 307(5713), 1270–1273. Retrieved
 544 from <http://www.sciencemag.org/content/307/5713/1270.long> doi:
 545 10.1126/science.1105978
- 546 Krimigis, S. M., Mitchell, D. G., Hamilton, D. C., Livi, S., Dandouras, J., Jaskulek,
 547 S., ... Williams, D. J. (2004). Magnetosphere Imaging Instrument (MIMI)
 548 on the Cassini mission to Saturn/Titan. *Space Science Reviews*, 114(1-4),
 549 233–329. doi: 10.1007/s11214-004-1410-8
- 550 Krimigis, S. M., Sergis, N., Mitchell, D. G., Hamilton, D. C., & Krupp, N. (2007).
 551 A dynamic, rotating ring current around Saturn. *Nature*, 450(7172), 1050–
 552 1053. Retrieved from <https://www.nature.com/articles/nature06425> doi:
 553 10.1038/nature06425
- 554 Lamy, L. (2017). The Saturnian Kilometric Radiation before the Cassini Grand Fi-
 555 nale. In *Proceedings of the 8th international workshop on planetary, solar and*
 556 *heliospheric radio emissions (pre viii)*. Seggau, Austria. Retrieved from
 557 <http://arxiv.org/abs/1709.07693>
- 558 Lamy, L., Prangé, R., Pryor, W., Gustin, J., Badman, S. V., Melin, H., ... Brandt,
 559 P. C. (2013). Multispectral simultaneous diagnosis of Saturn's aurorae
 560 throughout a planetary rotation. *Journal of Geophysical Research: Space*
 561 *Physics*, 118(8), 4817–4843. Retrieved from [http://onlinelibrary.wiley](http://onlinelibrary.wiley.com/doi/10.1002/jgra.50404/abstract)
 562 [.com/doi/10.1002/jgra.50404/abstract](http://onlinelibrary.wiley.com/doi/10.1002/jgra.50404/abstract) doi: 10.1002/jgra.50404
- 563 Lazarus, A. J., & McNutt, R. L. (1983). Low-Energy Plasma Ion Observations

- 564 in Saturn's Magnetosphere. *Journal of Geophysical Research*, 88(A11), 8831–
 565 8846. Retrieved from [https://agupubs.onlinelibrary.wiley.com/doi/abs/](https://agupubs.onlinelibrary.wiley.com/doi/abs/10.1029/JA088iA11p08831)
 566 [10.1029/JA088iA11p08831](https://agupubs.onlinelibrary.wiley.com/doi/abs/10.1029/JA088iA11p08831) doi: 10.1029/JA088iA11p08831
- 567 Mauk, B. H., Allegrini, F., Bagenal, F., Bolton, S. J., Clark, G., Connerney, J. E.,
 568 ... Rymer, A. M. (2020). Energetic Neutral Atoms From Jupiter's Polar
 569 Regions. *Journal of Geophysical Research: Space Physics*, 125(12), 1–15.
 570 Retrieved from [https://agupubs.onlinelibrary.wiley.com/doi/full/](https://agupubs.onlinelibrary.wiley.com/doi/full/10.1029/2020JA028697?saml_referrer)
 571 [10.1029/2020JA028697?saml_referrer](https://agupubs.onlinelibrary.wiley.com/doi/full/10.1029/2020JA028697?saml_referrer) doi: 10.1029/2020JA028697
- 572 Mauk, B. H., Clark, G., Allegrini, F., Bagenal, F., Bolton, S. J., Connerney, J. E.,
 573 ... Rymer, A. M. (2020). Juno Energetic Neutral Atom (ENA) Remote Mea-
 574 surements of Magnetospheric Injection Dynamics in Jupiter's Io Torus Regions.
 575 *Journal of Geophysical Research: Space Physics*, 125(5), 1–15. Retrieved
 576 from [https://agupubs.onlinelibrary.wiley.com/doi/epdf/10.1029/](https://agupubs.onlinelibrary.wiley.com/doi/epdf/10.1029/2020JA027964)
 577 [2020JA027964](https://agupubs.onlinelibrary.wiley.com/doi/epdf/10.1029/2020JA027964) doi: 10.1029/2020JA027964
- 578 Mauk, B. H., Mitchell, D. G., Krimigis, S. M., Roelof, E. C., & Paranicas, C. P.
 579 (2003). Energetic neutral atoms from a trans-Europa gas torus at Jupiter.
 580 *Nature*, 421(6926), 920–922. Retrieved from [https://www.nature.com/](https://www.nature.com/articles/nature01431)
 581 [articles/nature01431](https://www.nature.com/articles/nature01431) doi: 10.1038/nature01431
- 582 McAndrews, H. J., Thomsen, M. F., Arridge, C. S., Jackman, C. M., Wilson,
 583 R. J., Henderson, M. G., ... Dougherty, M. K. (2009). Plasma in Saturn's
 584 nightside magnetosphere and the implications for global circulation. *Plan-*
 585 *etary and Space Science*, 57(14-15), 1714–1722. Retrieved from [https://](https://www.sciencedirect.com/science/article/pii/S0032063309000750#bib19)
 586 www.sciencedirect.com/science/article/pii/S0032063309000750#bib19
 587 doi: 10.1016/j.pss.2009.03.003
- 588 Melin, H., Shemansky, D. E., & Liu, X. (2009). The distribution of atomic hy-
 589 drogen and oxygen in the magnetosphere of Saturn. *Planetary and Space Sci-*
 590 *ence*, 57(14-15), 1743–1753. Retrieved from [http://dx.doi.org/10.1016/j](http://dx.doi.org/10.1016/j.pss.2009.04.014)
 591 [.pss.2009.04.014](http://dx.doi.org/10.1016/j.pss.2009.04.014) doi: 10.1016/j.pss.2009.04.014
- 592 Mitchell, D. G., Brandt, P. C., Carbary, J. F., Kurth, W. S., Krimigis, S. M., Paran-
 593 icas, C., ... Pryor, W. R. (2015). Injection, Interchange, and Reconnection:
 594 Energetic Particle Observations in Saturn's Magnetosphere. In A. Keiling,
 595 C. M. Jackman, & P. A. Delamere (Eds.), *Magnetotails in the solar system*
 596 (chap. 19). Hoboken, NJ: John Wiley and Sons, Inc. Retrieved from [http://](http://onlinelibrary.wiley.com/doi/10.1002/9781118842324.ch19/summary)
 597 onlinelibrary.wiley.com/doi/10.1002/9781118842324.ch19/summary
 598 doi: 10.1002/9781118842324.ch19
- 599 Mitchell, D. G., Brandt, P. C., Roelof, E. C., Dandouras, J., Krimigis, S. M., Mauk,
 600 B. H., ... Shemansky, D. E. (2005). Energetic ion acceleration in Saturn's
 601 magnetotail: Substorms at Saturn? *Geophysical Research Letters*, 32(20),
 602 1–4. Retrieved from [https://agupubs.onlinelibrary.wiley.com/doi/full/](https://agupubs.onlinelibrary.wiley.com/doi/full/10.1029/2005GL022647)
 603 [10.1029/2005GL022647](https://agupubs.onlinelibrary.wiley.com/doi/full/10.1029/2005GL022647) doi: 10.1029/2005GL022647
- 604 Mitchell, D. G., Krimigis, S. M., Paranicas, C., Brandt, P. C., Carbary, J. F.,
 605 Roelof, E. C., ... Pryor, W. R. (2009). Recurrent energization of plasma
 606 in the midnight-to-dawn quadrant of Saturn's magnetosphere, and its rela-
 607 tionship to auroral UV and radio emissions. *Planetary and Space Science*,
 608 57(14-15), 1732–1742. Retrieved from [http://www.sciencedirect.com/](http://www.sciencedirect.com/science/article/pii/S0032063309001044)
 609 [science/article/pii/S0032063309001044](http://www.sciencedirect.com/science/article/pii/S0032063309001044) doi: 10.1016/j.pss.2009.04.002
- 610 Mitchell, D. G., Kurth, W. S., Hospodarsky, G. B., Krupp, N., Saur, J., Mauk,
 611 B. H., ... Hamilton, D. C. (2009). Ion conics and electron beams associated
 612 with auroral processes on Saturn. *Journal of Geophysical Research: Space*
 613 *Physics*, 114(A02212). Retrieved from [https://agupubs.onlinelibrary](https://agupubs.onlinelibrary.wiley.com/doi/full/10.1029/2008JA013621)
 614 [.wiley.com/doi/full/10.1029/2008JA013621](https://agupubs.onlinelibrary.wiley.com/doi/full/10.1029/2008JA013621) doi: 10.1029/2008ja013621
- 615 Morooka, M. W., Modolo, R., Wahlund, J. E., André, M., Eriksson, A. I., Per-
 616 soon, A. M., ... Dougherty, M. (2009). The electron density of Sat-
 617 urn's magnetosphere. *Annales Geophysicae*, 27(7), 2971–2991. Retrieved
 618 from <https://angeo.copernicus.org/articles/27/2971/2009/> doi:

- 10.5194/angeo-27-2971-2009
- 619
620 Nichols, J. D., V. badman, S., Baines, K. H., Brown, R. H., Bunce, E. J., Clarke,
621 J. T., ... Stallard, T. S. (2014). Dynamic auroral storms on Saturn as ob-
622 served by the Hubble Space Telescope. *Geophysical Research Letters*, *41*(10),
623 3323–3330. Retrieved from [http://onlinelibrary.wiley.com/doi/10.1002/](http://onlinelibrary.wiley.com/doi/10.1002/2014GL060186/abstract)
624 [2014GL060186/abstract](http://onlinelibrary.wiley.com/doi/10.1002/2014GL060186) doi: 10.1002/2014GL060186
- 625 Palmaerts, B., Yao, Z. H., Sergis, N., Guo, R. L., Grodent, D., Dialynas, K.,
626 ... Mitchell, D. G. (2020). A Long-Lasting Auroral Spiral Rotat-
627 ing Around Saturn’s Pole. *Geophysical Research Letters*, *47*(23), 1–
628 10. Retrieved from [https://agupubs.onlinelibrary.wiley.com/](https://agupubs.onlinelibrary.wiley.com/doi/full/10.1029/2020GL088810?casa_token=7kvj3ezuX3YAAAAA%3AqGC-a4RIoN4-P2S-Pb6D1DFqyZrV1bL7eeiwG-sDyPf-A3dVsZT_Kp4YBmhFX9C3Rq7yay6Eoh8eT5JXSg)
629 [doi/full/10.1029/2020GL088810?casa_token=7kvj3ezuX3YAAAAA%](https://agupubs.onlinelibrary.wiley.com/doi/full/10.1029/2020GL088810?casa_token=7kvj3ezuX3YAAAAA%3AqGC-a4RIoN4-P2S-Pb6D1DFqyZrV1bL7eeiwG-sDyPf-A3dVsZT_Kp4YBmhFX9C3Rq7yay6Eoh8eT5JXSg)
630 [3AqGC-a4RIoN4-P2S-Pb6D1DFqyZrV1bL7eeiwG-sDyPf-A3dVsZT](https://agupubs.onlinelibrary.wiley.com/doi/full/10.1029/2020GL088810?casa_token=7kvj3ezuX3YAAAAA%3AqGC-a4RIoN4-P2S-Pb6D1DFqyZrV1bL7eeiwG-sDyPf-A3dVsZT_Kp4YBmhFX9C3Rq7yay6Eoh8eT5JXSg)
631 [_Kp4YBmhFX9C3Rq7yay6Eoh8eT5JXSg](https://agupubs.onlinelibrary.wiley.com/doi/full/10.1029/2020GL088810?casa_token=7kvj3ezuX3YAAAAA%3AqGC-a4RIoN4-P2S-Pb6D1DFqyZrV1bL7eeiwG-sDyPf-A3dVsZT_Kp4YBmhFX9C3Rq7yay6Eoh8eT5JXSg) doi: 10.1029/2020GL088810
- 632 Paranicas, C., Mitchell, D. G., Krimigis, S. M., Hamilton, D. C., Roussos, E.,
633 Krupp, N., ... Armstrong, T. P. (2008). Sources and losses of ener-
634 getic protons in Saturn’s magnetosphere. *Icarus*, *197*(2), 519–525. Re-
635 trieved from [https://www.sciencedirect.com/science/article/pii/](https://www.sciencedirect.com/science/article/pii/S0019103508002133)
636 [S0019103508002133](https://www.sciencedirect.com/science/article/pii/S0019103508002133) doi: 10.1016/j.icarus.2008.05.011
- 637 Paranicas, C., Mitchell, D. G., Roelof, E. C., Brandt, P. C., Williams, D. J., Krim-
638 igis, S. M., & Mauk, B. H. (2005). Periodic intensity variations in global ENA
639 images of Saturn. *Geophysical Research Letters*, *32*(21), 1–4. Retrieved from
640 <http://onlinelibrary.wiley.com/doi/10.1029/2005GL023656/full> doi:
641 [10.1029/2005GL023656](http://onlinelibrary.wiley.com/doi/10.1029/2005GL023656/full)
- 642 Paranicas, C., Thomsen, M. F., Kollmann, P., Azari, A. R., Bader, A., Bad-
643 man, S. V., ... Roussos, E. (2020). Inflow Speed Analysis of Inter-
644 change Injections in Saturn’s Magnetosphere. *Journal of Geophysical Re-*
645 *search: Space Physics*, *125*(9), e2020JA028299. Retrieved from [https://](https://agupubs.onlinelibrary.wiley.com/doi/10.1029/2020JA028299)
646 agupubs.onlinelibrary.wiley.com/doi/10.1029/2020JA028299 doi:
647 [10.1029/2020JA028299](https://agupubs.onlinelibrary.wiley.com/doi/10.1029/2020JA028299)
- 648 Provan, G., Andrews, D. J., Arridge, C. S., Coates, a. J., Cowley, S. W. H., Cox,
649 G., ... Jackman, C. M. (2012). Dual periodicities in planetary-period mag-
650 netic field oscillations in Saturn’s tail. *Journal of Geophysical Research: Space*
651 *Physics*, *117*(1), 1–20. Retrieved from [http://onlinelibrary.wiley.com/](http://onlinelibrary.wiley.com/doi/10.1029/2011JA017104/abstract)
652 [doi/10.1029/2011JA017104/abstract](http://onlinelibrary.wiley.com/doi/10.1029/2011JA017104/abstract) doi: 10.1029/2011JA017104
- 653 Provan, G., Cowley, S. W. H., Lamy, L., Bunce, E. J., Hunt, G. J., Zarka, P., &
654 Dougherty, M. K. (2016). Planetary period oscillations in Saturn’s magne-
655 tosphere: Coalescence and reversal of northern and southern periods in late
656 northern spring. *Journal of Geophysical Research: Space Physics*, *121*, 9829–
657 9862. Retrieved from [http://onlinelibrary.wiley.com/doi/10.1002/](http://onlinelibrary.wiley.com/doi/10.1002/2016JA023056/full)
658 [2016JA023056/full](http://onlinelibrary.wiley.com/doi/10.1002/2016JA023056/full) doi: 10.1002/2016JA023056
- 659 Ramer, K. M., Kivelson, M. G., Sergis, N., Khurana, K. K., & Jia, X. (2017). Spin-
660 ning, breathing, and flapping: Periodicities in Saturn’s middle magnetosphere.
661 *Journal of Geophysical Research: Space Physics*, *122*(1), 393–416. Retrieved
662 from [https://agupubs.onlinelibrary.wiley.com/doi/full/10.1002/](https://agupubs.onlinelibrary.wiley.com/doi/full/10.1002/2016JA023126)
663 [2016JA023126](https://agupubs.onlinelibrary.wiley.com/doi/full/10.1002/2016JA023126) doi: 10.1002/2016JA023126
- 664 Richardson, J. D., Eviatar, A., McGrath, M. A., & Vasyliūnas, V. M. (1998, aug).
665 OH in Saturn’s magnetosphere: Observations and implications. *Journal*
666 *of Geophysical Research: Planets*, *103*(E9), 20245–20255. Retrieved from
667 <http://doi.wiley.com/10.1029/98JE01127> doi: 10.1029/98JE01127
- 668 Roelof, E. C. (1987, jun). Energetic neutral atom image of a storm-time
669 ring current. *Geophysical Research Letters*, *14*(6), 652–655. Retrieved
670 from [https://agupubs.onlinelibrary.wiley.com/doi/abs/10.1029/](https://agupubs.onlinelibrary.wiley.com/doi/abs/10.1029/GL014i006p00652)
671 [GL014i006p00652](https://agupubs.onlinelibrary.wiley.com/doi/abs/10.1029/GL014i006p00652)<http://doi.wiley.com/10.1029/GL014i006p00652> doi:
672 [10.1029/GL014i006p00652](https://agupubs.onlinelibrary.wiley.com/doi/abs/10.1029/GL014i006p00652)
- 673 Roelof, E. C., Mitchell, D. G., & Williams, D. J. (1985). Energetic neutral atoms (E

- 674 ~ 50 keV) from the ring current: IMP 7/8 and ISEE 1. *Journal of Geophysical*
675 *Research*, 90(A11), 10991. Retrieved from [http://doi.wiley.com/10.1029/](http://doi.wiley.com/10.1029/JA090iA11p10991)
676 [JA090iA11p10991](http://doi.wiley.com/10.1029/JA090iA11p10991) doi: 10.1029/JA090iA11p10991
- 677 Roelof, E. C., & Skinner, A. J. (2000). Extraction of ion distributions from magne-
678 toospheric ENA and EUV images. *Space Sci. Rev.*, 91(1-2), 437–459. Retrieved
679 from <https://link.springer.com/article/10.1023/A:1005281424449> doi:
680 10.1023/A:1005281424449
- 681 Roussos, E., Kollmann, P., Krupp, N., Paranicas, C., Dialynas, K., Jones, G. H., ...
682 Cooper, J. F. (2019). Sources, Sinks, and Transport of Energetic Electrons
683 Near Saturn’s Main Rings. *Geophysical Research Letters*, 46(7), 3590–3598.
684 Retrieved from [https://agupubs.onlinelibrary.wiley.com/doi/full/](https://agupubs.onlinelibrary.wiley.com/doi/full/10.1029/2018GL078097)
685 [10.1029/2018GL078097](https://agupubs.onlinelibrary.wiley.com/doi/full/10.1029/2018GL078097) doi: 10.1029/2018GL078097
- 686 Sergis, N., Krimigis, S. M., Mitchell, D. G., Hamilton, D. C., Krupp, N., Mauk,
687 B. M., ... Dougherty, M. (2007). Ring current at Saturn: Energetic
688 particle pressure in Saturn’s equatorial magnetosphere measured with
689 Cassini/MIMI. *Geophysical Research Letters*, 34(9), 1–6. Retrieved from
690 <http://onlinelibrary.wiley.com/doi/10.1029/2006GL029223/full> doi:
691 10.1029/2006GL029223
- 692 Sun, Y. X., Roussos, E., Krupp, N., Zong, Q. G., Kollmann, P., & Zhou,
693 X. Z. (2019). Spectral Signatures of Adiabatic Electron Acceleration
694 at Saturn Through Corotation Drift Cancellation. *Geophysical*
695 *Research Letters*, 46(17-18), 10240–10249. Retrieved from [https://](https://agupubs.onlinelibrary.wiley.com/doi/full/10.1029/2019GL084113)
696 agupubs.onlinelibrary.wiley.com/doi/full/10.1029/2019GL084113
697 [?casa_token=1kBOPhr7xPkAAAAA%3AL6NJsFyw6ceo6Lg_wYjKNvvpk](https://agupubs.onlinelibrary.wiley.com/doi/full/10.1029/2019GL084113?casa_token=1kBOPhr7xPkAAAAA%3AL6NJsFyw6ceo6Lg_wYjKNvvpk_tzn5cu5LZH1nDTq3gbapTDND3jjZgZEBVyxtXPrhwTMdvdIFbfxf-cSLw)
698 [_tzn5cu5LZH1nDTq3gbapTDND3jjZgZEBVyxtXPrhwTMdvdIFbfxf-cSLw](https://agupubs.onlinelibrary.wiley.com/doi/full/10.1029/2019GL084113?casa_token=1kBOPhr7xPkAAAAA%3AL6NJsFyw6ceo6Lg_wYjKNvvpk_tzn5cu5LZH1nDTq3gbapTDND3jjZgZEBVyxtXPrhwTMdvdIFbfxf-cSLw) doi:
699 10.1029/2019GL084113
- 700 Thomsen, M. F., Jackman, C. M., Cowley, S. W., Jia, X., Kivelson, M. G., &
701 Provan, G. (2017). Evidence for periodic variations in the thickness of Sat-
702 urn’s nightside plasma sheet. *Journal of Geophysical Research: Space Physics*,
703 122(1), 280–292. Retrieved from [http://onlinelibrary.wiley.com/doi/](http://onlinelibrary.wiley.com/doi/10.1002/2016JA023368/full)
704 [10.1002/2016JA023368/full](http://onlinelibrary.wiley.com/doi/10.1002/2016JA023368/full) doi: 10.1002/2016JA023368
- 705 Thomsen, M. F., Jackman, C. M., Tokar, R. L., & Wilson, R. J. (2014). Plasma
706 flows in Saturn’s nightside magnetosphere. *Journal of Geophysical Research:*
707 *Space Physics*, 119, 4521–4535. Retrieved from [http://onlinelibrary.wiley](http://onlinelibrary.wiley.com/doi/10.1002/2014JA019912/abstract)
708 [.com/doi/10.1002/2014JA019912/abstract](http://onlinelibrary.wiley.com/doi/10.1002/2014JA019912/abstract) doi: 10.1002/2014JA019912
- 709 Thomsen, M. F., Mitchell, D. G., Jia, X., Jackman, C. M., Hospodarsky, G., &
710 Coates, A. J. (2015). Plasmopause formation at Saturn. *Journal of*
711 *Geophysical Research: Space Physics*, 120, 2571–2583. Retrieved from
712 <http://onlinelibrary.wiley.com/doi/10.1002/2015JA021008/abstract>
713 doi: 10.1002/2015JA021008
- 714 Thomsen, M. F., Roussos, E., Andriopoulou, M., Kollmann, P., Arridge, C. S., Paran-
715 icas, C. P., ... Young, D. T. (2012). Saturn’s inner magnetospheric convection
716 pattern: Further evidence. *Journal of Geophysical Research: Space Physics*,
717 117(9), 1–19. Retrieved from [https://agupubs.onlinelibrary.wiley.com/](https://agupubs.onlinelibrary.wiley.com/doi/full/10.1029/2011JA017482)
718 [doi/full/10.1029/2011JA017482](https://agupubs.onlinelibrary.wiley.com/doi/full/10.1029/2011JA017482) doi: 10.1029/2011JA017482
- 719 Wilson, R. J., Bagenal, F., Delamere, P. A., Desroche, M., Fleshman, B. L.,
720 & Dols, V. (2013). Evidence from radial velocity measurements of a
721 global electric field in Saturn’s inner magnetosphere. *Journal of Geo-*
722 *physical Research: Space Physics*, 118(5), 2122–2132. Retrieved from
723 <https://agupubs.onlinelibrary.wiley.com/doi/10.1002/jgra.50251>
724 doi: 10.1002/jgra.50251
- 725 Wilson, R. J., Bagenal, F., & Persoon, A. M. (2017). Survey of thermal plasma
726 ions in Saturn’s magnetosphere utilizing a forward model. *Journal of Geophys-*
727 *ical Research: Space Physics*, 122(7), 7256–7278. Retrieved from [https://](https://agupubs.onlinelibrary.wiley.com/doi/full/10.1002/2017JA024117)
728 agupubs.onlinelibrary.wiley.com/doi/full/10.1002/2017JA024117 doi:

729
730
731
732
733
734
735
736
737
738

10.1002/2017JA024117
Wing, S., Brandt, P. C., Mitchell, D. G., Johnson, J. R., Kurth, W. S., & Menietti, J. D. (2020). Periodic Narrowband Radio Wave Emissions and Inward Plasma Transport at Saturn's Magnetosphere. *The Astronomical Journal*, *159*(6), 249. Retrieved from <https://iopscience.iop.org/article/10.3847/1538-3881/ab818d/pdf> doi: 10.3847/1538-3881/ab818d
Ye, S. Y., Fischer, G., Kurth, W. S., Menietti, J. D., & Gurnett, D. A. (2016). Rotational modulation of Saturn's radio emissions after equinox. *Journal of Geophysical Research: Space Physics*, *121*. Retrieved from <http://onlinelibrary.wiley.com/doi/10.1002/2016JA023281/full> doi: 10.1002/2016JA023281